Cascade time scales for energy and helicity in homogeneous isotropic turbulence

Susan Kurien

Center for Nonlinear Studies and Theoretical Division, Los Alamos National Laboratory, Los Alamos, New Mexico 87545, USA

Mark A. Taylor

Computer and Computational Sciences Division, Los Alamos National Laboratory, Los Alamos, New Mexico 87545, USA

Takeshi Matsumoto

Department of Physics, Kyoto University, Kitashirakawa Oiwakecho Sakyo-ku, Kyoto 606-8502, Japan

We extend the Kolmogorov phenomenology for the scaling of energy spectra in high-Reynolds-number turbulence, to explicitly include the effect of helicity. There exists a time scale τ_H for helicity transfer in homogeneous, isotropic turbulence with helicity. We arrive at this time scale using the phenomenological arguments used by Kraichnan to derive the time scale τ_E for energy transfer [R. H. Kraichnan, J. Fluid Mech. **47**, 525 (1971)]. We show that in general τ_H may not be neglected compared to τ_E, even for rather low relative helicity. We then deduce an inertial range joint cascade of energy and helicity in which the dynamics are dominated by τ_E in the low wave numbers with both energy and helicity spectra scaling as $k^{-5/3}$; and by τ_H at larger wave numbers with spectra scaling as $k^{-4/3}$. We demonstrate how, within this phenomenology, the commonly observed "bottleneck" in the energy spectrum might be explained. We derive a wave number k_h which is less than the Kolmogorov dissipation wave number, at which both energy and helicity cascades terminate due to dissipation effects. Data from direct numerical simulations are used to check our predictions.

Energy and helicity [1,2] are the two known inviscid invariants of the Navier–Stokes equations. It was postulated in Ref. [3] that in isotropic flows with helicity, these quantities cascade together from large to small scales. This joint forward cascade of energy and helicity has been verified by direct numerical simulations, most recently at a resolution of 512^3 grid points [4]. Kraichnan [5] defined the shear time scale τ_E for energy transfer, based solely on energy dynamics. Assuming that helicity dynamics are also controlled by τ_E, a $k^{-5/3}$ inertial range scaling was established for both energy and helicity spectra [3].

We would first like to ascribe spatial geometrical properties to the types of quantities used to derive the relevant time scales. We recall the spectral formulation $\langle \tilde{u}_i(\mathbf{k})\tilde{u}_j^*(\mathbf{k})\rangle$ of the two-point velocity correlation function in isotropic, homogeneous, statistically stationary turbulence. It may be decomposed into its index-symmetric and index-antisymmetric parts as

$$E_{ij}(\mathbf{k}) = \tfrac{1}{2}[\langle \tilde{u}_i(\mathbf{k})\tilde{u}_j^*(\mathbf{k})\rangle + \langle \tilde{u}_j(\mathbf{k})\tilde{u}_i^*(\mathbf{k})\rangle], \qquad (1)$$

$$\tilde{E}_{ij}(\mathbf{k}) = \tfrac{1}{2}[\langle \tilde{u}_i(\mathbf{k})\tilde{u}_j^*(\mathbf{k})\rangle - \langle \tilde{u}_j(\mathbf{k})\tilde{u}_i^*(\mathbf{k})\rangle], \qquad (2)$$

where $\tilde{\mathbf{u}}_i = \tilde{u}_i\hat{\mathbf{i}}$ and $\tilde{u}_i$ is the magnitude of the ith component of the velocity vector in a chosen Cartesian coordinate system. Equation (1) when contracted with the projection operator $\delta_{ij}/2$ and then averaged over $\hat{\mathbf{k}}$ gives the energy spectrum $E(k)$. It is therefore clear that the types of correlations contributing to $E(k)$ are those in which $i=j$ and hence $\hat{\mathbf{i}}, \hat{\mathbf{j}}$ and the unit wave vector $\hat{\mathbf{k}}$ all lie in the same plane. The corresponding picture in real space is to consider the index-symmetric

two-point spatial correlation functions $R_{ij}^S(\mathbf{r}) = \tfrac{1}{2}\langle u_i(\mathbf{x})u_j(\mathbf{x}+\mathbf{r}) + u_j(\mathbf{x})u_i(\mathbf{x}+\mathbf{r})\rangle$ which has the tensor representation $\sim A(r)\delta_{ij} + B(r)(r_i r_j/r^2)$ for the isotropic case; the incompressibility constraint gives a relationship between $A(r)$ and $B(r)$. This index-symmetric correlation function thus has nonzero contributions when $\hat{\mathbf{i}}, \hat{\mathbf{j}}$, and $\hat{\mathbf{r}}$ are co-planar. We will refer to these as "in-plane" correlations (see Fig. 1 for a sketch of these types of isotropic correlations). Similarly, Eq. (2) when contracted with the antisymmetric curl operator $\hat{i}\varepsilon_{ijl}k_l$, where $\hat{i}=\sqrt{-1}$, and then averaged over $\hat{\mathbf{k}}$ gives the total helicity density $H(k)=2k\tilde{E}(k)$. [Note that this relationship is distinct from the Schwartz inequality $|H(k)| \leqslant 2kE(k)$.] Therefore the types of correlations contributing to $\tilde{E}_{ij}(k)$ [and hence to $H(k)$] are those in which $\hat{\mathbf{i}}, \hat{\mathbf{j}}$, and unit wave vector $\hat{\mathbf{k}}$ are mutually orthogonal. Again, the corresponding formulation in real space is the index-antisymmetric two-point spatial correlation functions $R_{ij}^A(\mathbf{r}) = \tfrac{1}{2}\langle u_i(\mathbf{x})u_j(\mathbf{x}+\mathbf{r}) - u_j(\mathbf{x})u_i(\mathbf{x}+\mathbf{r})\rangle$ which has the tensor representation $\sim \varepsilon_{ijl}r_l/r$ and thus has nonzero contributions when $\hat{\mathbf{i}}, \hat{\mathbf{j}}$, and $\hat{\mathbf{r}}$ are mutually or-
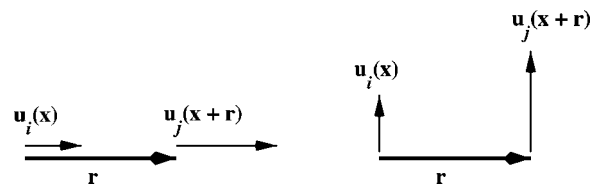

FIG. 1. The in-plane longitudinal and transverse correlation configurations which contribute to the isotropic symmetric correlation function $R_{ij}^S(\mathbf{r})$.
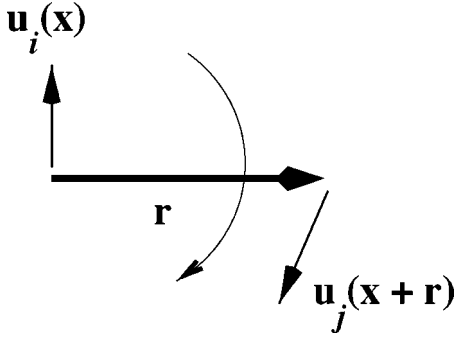
FIG. 2. The out-of-plane correlation configuration which contributes to the isotropic antisymmetric correlation function $R_{ij}^A(\mathbf{r})$. The intrinsic "handedness" of this configuration, indicated by the curved arrow, cannot appear in the geometry of Fig. 1.

thogonal to each other (see Fig. 2 for a sketch). We will refer to these as "out-of-plane" correlations. Here $E(k) = \Sigma_{|\mathbf{k}|=k} \frac{1}{2}|\tilde{\mathbf{u}}(\mathbf{k})|^2$ and $H(k) = \Sigma_{|\mathbf{k}|=k} \tilde{\mathbf{u}}(\mathbf{k}) \cdot \tilde{\omega}(-\mathbf{k})$ where $\tilde{\mathbf{u}}(\mathbf{k})$ and $\tilde{\omega}(\mathbf{k})$ are the Fourier transforms of the velocity $\mathbf{u}(\mathbf{x})$ and the vorticity $\boldsymbol{\omega}(\mathbf{x}) = \nabla \times \mathbf{u}(\mathbf{x})$, respectively.

The Kraichnan time scale for energy transfer τ_E corresponds to correlations of the type $E_{ij}(\mathbf{k})$ [Eq. (1)] which arise due to shearing motions in the plane of coordinates i, j, and unit wave number $\hat{\mathbf{k}}$ [5]. Such in-plane shearing motions cannot give rise to correlations of the type $\tilde{E}_{ij}(\mathbf{k})$ [Eq. (2)] which relate orthogonal components $u_i\hat{\mathbf{i}}$ and $u_j\hat{\mathbf{j}}$ across the third mutually orthogonal direction $\hat{\mathbf{k}}$. For this we require out-of-plane shearing motions as depicted in Fig. 2, which are provided by the presence of helicity [6,7]. We first derive the time scale τ_H, associated with such an out-of-plane shear. The governing factor is the relative helicity $|H(k)|/[2kE(k)]$ which will be shown to fall off linearly in wave number restoring parity as k becomes very large. Crucially, we will show that the ratio $\tau_E/\tau_H \sim \{|H(k)|/[2kE(k)]\}^{1/2}$, which decays slower than the relative helicity. Therefore the effect of τ_H cannot be neglected. We demonstrate the effect of this new time scale on energy and helicity spectra, and offer an interpretation of the "bottleneck" effect observed in measured energy spectra. Finally, the new dynamics reveal a dissipation scale which is larger than the Kolmogorov dissipation scale, suggesting that the joint cascade is truncated sooner in wave-number space if helicity is present.

We performed two simulations of the three-dimensional (3D), forced Navier-Stokes equation in a unit-periodic box with 512 (data I), and 1024 (data II) grid points to a side, respectively. In these units, the wave number k is in integer multiples of 2π. Energy and helicity were injected into the

flow for $k \leq 2$ at each time step. The forcing scheme was the same as in Ref. [8]. For case I we imposed maximum helicity in $k \leq 2$ [4,9], resulting in a mean helicity over time of -26.8 in the units of our simulation. For case II the helicity input was uncontrolled and random, resulting in a mean helicity of -0.12 which is essentially zero compared to case I. The spectra for case I were averaged over 40 snapshots spanning eight large-eddy turnover times after spin up. The spectra for case II were averaged over 48 snapshots spanning two large-eddy turnover times after spin up. The spin up time in each case was defined to be when the input rate of energy matched the dissipation rate of energy, the flow having achieved statistically steady state. Additional parameters of the simulations are given in Table I.

We recall the introduction in Ref. [5] of the distortion time scale (or eddy-turnover time) of an eddy with wave number k,

$$\tau_E^2 \sim \left(\int_0^k E(p)p^2 dp \right)^{-1} \sim [E(k)k^3]^{-1}, \qquad (3)$$

where Kraichnan assumes that only wave numbers $\leq k$ will have a shearing action on wave numbers of order k; the effects from wave numbers $> k$ will average out. Notice that the local shear time scale thus defined depends on the in-plane correlations which contribute to the energy spectrum as described above. Analogously, we can define the time scale τ_H for out-of-plane distortions of an eddy, from the antisymmetric co-spectrum,

$$\tau_H^2 \sim \left(\int_0^k |\tilde{E}(p)|p^2 dp \right)^{-1} \sim \left(\frac{1}{2}|H(k)|k^2 \right)^{-1}. \qquad (4)$$

The distortion or shear corresponding to τ_H is different from the distortion corresponding to τ_E of Ref. [5]. The shear in the former case derives from the out-of-plane correlations contributing to the antisymmetric co-spectrum and hence to the helicity spectrum. The shear motion in this case is an out-of-plane twist for which the time scale is different than the in-plane shear rate corresponding to τ_E.

We estimate the transfer rate (flux) of helicity through wave number k, $F_H(k) \sim k|H(k)|/\tau_H \sim k^2|H(k)|^{3/2}$. Assuming steady-state, inertial range behavior with constant flux of helicity $F_H(k) = h$, the mean helicity dissipation rate, we obtain

$$H(k) \approx h^{2/3}k^{-4/3}. \qquad (5)$$

We compare τ_H with the time scale for energy transfer of

TABLE I. Parameters of the numerical simulations I and II. ν is the viscosity; R_λ is the Taylor-Reynolds number; mean total energy $E = \frac{1}{2}\Sigma_k \tilde{\mathbf{u}}(\mathbf{k})^2$; ε is the mean energy dissipation rate; mean total helicity $H = \Sigma_k \tilde{\mathbf{u}}(\mathbf{k}) \cdot \tilde{\omega}(-\mathbf{k})$; h is the mean helicity dissipation rate; $\eta_\varepsilon = (\nu^3/\varepsilon)^{1/4}$; $\eta_h = (\nu^3/h)^{1/5}$.

	N	ν(units of 10^4)	R_λ	E	ε	H	h	η_ε(units of 10^3)	η_h(units of 10^4)
I	512	1	270	1.72	1.51	-26.8	62.2	1.7	9
II	1024	0.35	430	1.87	1.75	-0.12	13.2	1.3	4

Eq. (3),

$$\frac{\tau_E}{\tau_H} \sim \left(\frac{|H(k)|}{2kE(k)} \right)^{1/2}. \qquad (6)$$

Since $\{|H(k)|/[2kE(k)]\}^{1/2} \gg |H(k)|/[2kE(k)]$ as the latter tends to zero, Eq. (6) implies that even for small values of the relative helicity, the time scales can become comparable. This is a fundamental point of difference from previous works in which the presence of helicity was considered inconsequential [3]. In previous arguments the fact that relative helicity must go to zero as $1/k$ in wave-number space meant that helicity could not have an effect on the long term dynamics since it must eventually be dominated by energy, restoring parity. Our present analysis shows that while the relative helicity does indeed go rapidly to zero, the relative *time scale* of helicity and energy transfer vanishes much more slowly. In other words, while the energy time scale is always faster, because of the Schwartz equality, the helicity time scale can remain comparable to it well into the large wave numbers. (For the initial value problems (decaying turbulence), the evolution equation of the relative helicity $H(k)/[2kE(k)]$ and its analytical bounds can be found in Ref. [10].)

With this second time scale at hand, we can now justifiably ask what the effect of τ_H will be on the energy spectrum. The energy flux ε through wave number k is

$$\varepsilon \sim \frac{kE(k)}{\tau_H} \sim kE(k)H(k)^{1/2}k. \qquad (7)$$

Using Eq. (5) in Eq. (7), we get

$$E(k) \approx \varepsilon h^{-1/3} k^{-4/3}. \qquad (8)$$

To summarize thus far, the τ_E dynamics result in Kolmogorov $k^{-5/3}$ scaling in both energy and helicity spectra, whereas τ_H dynamics result in $k^{-4/3}$ scaling in both. Clearly, the steeper $k^{-5/3}$ scaling should dominate in the low wave numbers while the $k^{-4/3}$ should manifest in the higher wave numbers. We emphasize that in order for the latter scaling to be visible in the high wave numbers, τ_H cannot be too much slower than τ_E. As shown above, according to Eq. (6), this may occur for very modest relative helicity in the high wave numbers, contrary to previous assumptions. The main point of our paper is that in general, the helicity time scale τ_H may not be ignored.

Figure 3 shows the energy and helicity spectra from our simulations. Each of the spectra is compensated by $k^{4/3}$ and by $k^{5/3}$ in order to distinguish the dominant scaling. For the strongly helical case I, there is good agreement with $k^{-4/3}$ scaling for both the energy and helicity spectra in approximately the same range [Figs. 3(a) and 3(b)] of slightly less than a decade. Note that the compensation with $k^{5/3}$ results in the commonly observed bottleneck phenomenon which we will discuss below. The energy spectrum of II [Fig. 3(c)] shows a range of $k^{-5/3}$ scaling followed by a range of $k^{-4/3}$ scaling (which appears as a bottleneck in the $k^{-5/3}$ compensated plot). The scaling ranges are modest even at this high resolution of 1024^3, but nonetheless the results are telling;

the scaling is most certainly not $k^{-5/3}$ throughout and the agreement with $k^{-4/3}$ though over a short range, certainly indicates shallower than $k^{-5/3}$ scaling behavior of the bottleneck region. The relative helicities in the range $10 < k < 100$, where the $k^{-4/3}$ scaling is seen, are shown in Fig. 4. For I, the relative helicity falls from about 10% to about 3% corresponding to τ_E/τ_H ranging from 32% to 17% according to Eq. (6). Despite the negligibly small total helicity $H = -0.12$ of II, and its noisy helicity spectrum (not shown), its relative helicity values lie between 1% and 5%. This implies that τ_E/τ_H could be as much as 22%. In both cases τ_H might in fact not be much longer than τ_E. It is important at this stage to comment on the appearance of a helicity-dependent scaling feature in flow II which is nominally helicity free on average. The first point is that zero average helicity does not imply that the average helicity spectrum $H(k)$ is zero for all k. In fact, we only input energy and helicity in the low wave numbers, the Navier-Stokes dynamics determines the helicity in all other wave numbers, including the highest wave numbers where in fact there is the well-known viscous helicity production. There is therefore no control of the helicity in a given wave number and the spectrum is generally not zero everywhere. The second point is that our analysis shows that it is not the total helicity but the *relative* helicity which determines the tradeoff between the two time scales. Given these two points it is not contradictory to measure $k^{-4/3}$ spectral scaling in the flow with negligible mean helicity. In fact, this flow is probably more similar to most experimental flows which are close to helicity free in the mean but with uncontrolled and often unknown helicity spectra [11].

These results are the first indication of the possibility of $k^{-4/3}$ scaling ranges in both energy and helicity spectra simultaneously. The possibility of a "pure" or "maximal" forward cascade of helicity scaling as $k^{-4/3}$ [3] with inverse cascade of energy scaling as $k^{-7/3}$ does not arise. This is because in our analysis we have retained the effect of the helical time scale τ_H and allowed it to modify the spectral dynamics. Since the scaling corresponding to τ_H is $k^{-4/3}$, a slower decay than $k^{-5/3}$, its "signature" in the spectra can dominate at large k even as the overall parity is being restored.

Based on the analysis above, we propose that the bottleneck in the total energy spectrum is in fact a *change in the scaling* of the energy spectrum, from a $k^{-5/3}$ regime in which the τ_E dynamics dominate to a less steep $k^{-4/3}$ regime in which the τ_H dynamics become significant. We will use the kinematic arguments of Ref. [12] with our new phenomenology and dynamics to analyze the bottleneck for such a helical influence. In simulations, it is possible to compute the total energy spectrum $E(k) = (1/2)\sum_{|\mathbf{k}|=k} |\tilde{\mathbf{u}}(\mathbf{k})|^2$ as a sum over a shell of radius k rather accurately. In experiments it is convenient to measure the one-dimensional (1D) longitudinal and transverse spectra along the measurement direction, say z. In our 3D flow simulation we calculate the 1D spectra as follows. The 1D Fourier transform in the z direction of the velocity $\mathbf{u}(\mathbf{x})$ is $\tilde{\tilde{\mathbf{u}}}(x,y,k_z) = (1/N)\sum_{n=1}^{N} e^{ik_z z_n} \mathbf{u}(x,y,z_n)$ where $0 \leq k_z \leq \pi/\delta z$. The longitudinal (transverse) 1D spectrum, averaged over the $x-y$ plane, is defined by
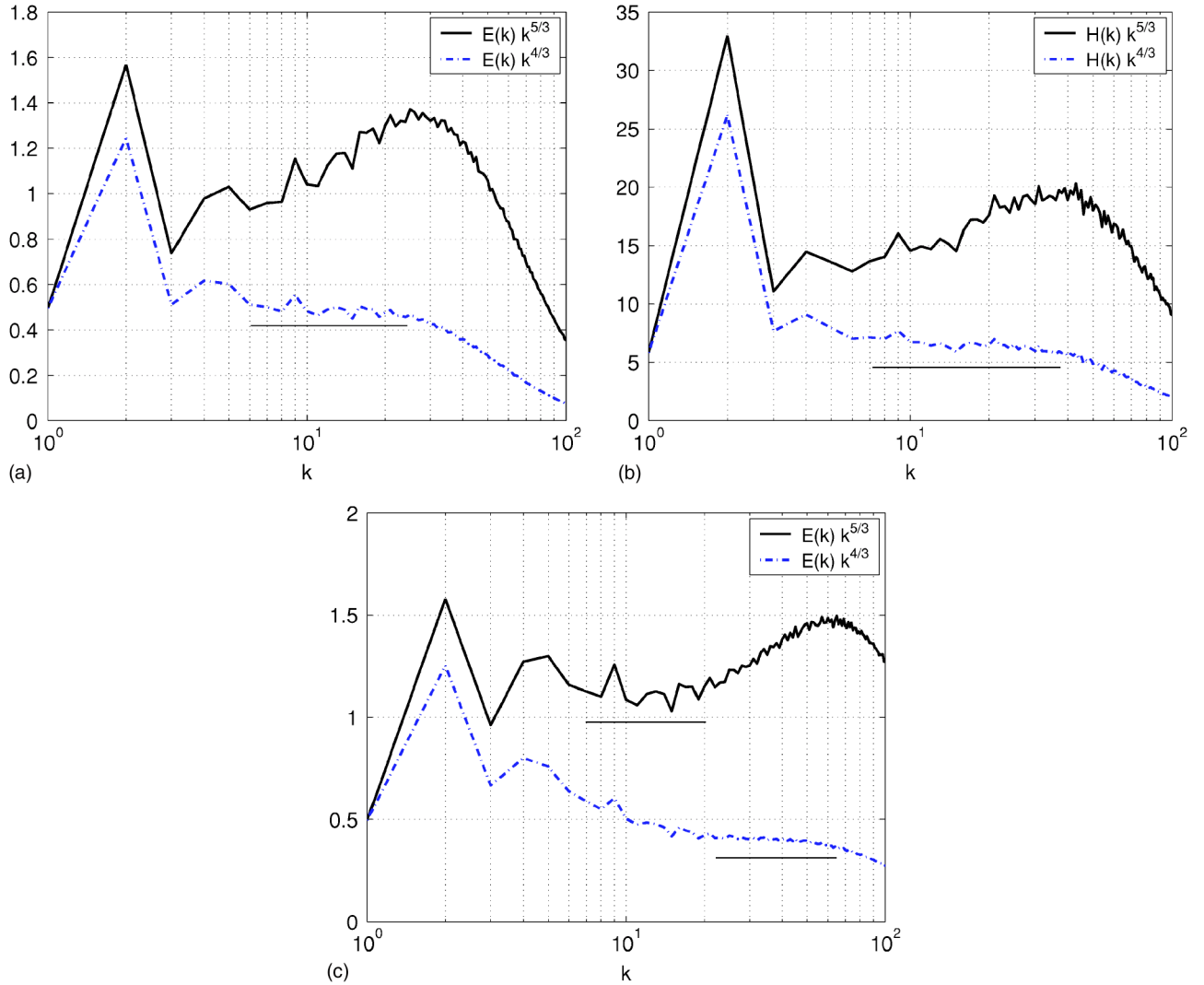
FIG. 3. Compensated spectra of (a) energy and (b) helicity, for data I. Observe the $k^{-4/3}$ scaling (dashed curve) range indicated by the horizontal line segment. (c) Compensated energy spectrum for data II. The horizontal line segments indicate ranges of $k^{-5/3}$ (solid curve) and $k^{-4/3}$ (dashed curve) scaling.

$$E_{L(T)}(k_z) = \frac{1}{(2N^2)} \sum_{p,q=1}^{N} |\widetilde{\widetilde{u}}_{z(\perp)}(x_p, y_q, k_z)|^2, \qquad (9)$$

where $|\widetilde{\widetilde{u}}_{\perp}|^2 = |\widetilde{\widetilde{u}}_x|^2 + |\widetilde{\widetilde{u}}_y|^2$. In isotropic flow, the 1D spectra should be independent of the direction in which the Fourier transform is performed. Our time-averaged longitudinal spectra computed in the the x, y, and z directions all collapse and the transverse spectra do the same. We average the 1D spectra in the three coordinate directions and drop the use of the subscript z to denote the direction of the Fourier transform. In isotropic flow there is a relation between the 1D and 3D spectra [12,13],

$$E(k) = -k\left(\frac{dE_L}{dk} + 2\frac{dE_T}{dk}\right). \qquad (10)$$

Our spectra satisfy Eq. (10) very well for $k \gtrsim 10$ and fairly well in the lower wave numbers. As emphasized in Ref. [12], Eq. (10) is a local relationship, wherein the functional form

of the total spectrum $E(k)$ is fully determined by the local behavior of E_L and E_T at a given wave number. For homogeneous, isotropic flows with helicity, it is reasonable to suppose that $E_L(k)$ [see the definition in Eq. (9)] would mainly carry contributions from the in-plane shear time scale τ_E. However, $E_T(k)$, which is related to the transverse components of the velocity Fourier transform, could be influenced by τ_H dynamics coming from $\widetilde{E}(k)$. The correlation time between transverse components can be slowed down by the dynamics of $\widetilde{E}(k)$ which arise due to the presence of helicity. Such coupling may not be deduced from kinematic arguments; it requires proper consideration of the new dynamics. Furthermore, it is not possible to see this coupling in the unclosed lowest-order Kármán-Howarth dyanamical equations wherein the symmetric and antisymmetric parts completely decouple for homogeneous flows [7]. It was pointed out in Ref. [6] that higher-order statistical equations for helical turbulence should show the coupling. The coupling is
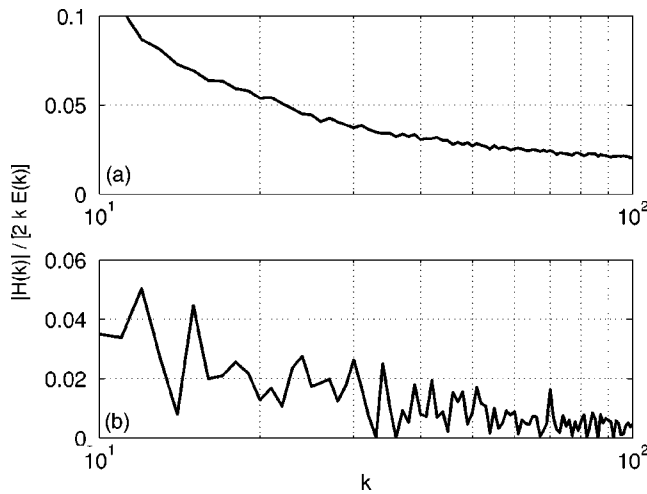
FIG. 4. The relative helicities for (a) data I and (b) data II, in the range $10 < k < 100$, where Fig. 3 shows $k^{-4/3}$ scaling. The relative helicity lies between 3% and 10% in (a) and between 1% and 5% in (b). The corresponding ratio of time scales τ_E/τ_H [Eq. (6)] is estimated to be up to 32% for data I, up to 22% for data II.

seen explicitly in the Eddy damped quasinormal Markovian (EDQNM) closure [14].

Figure 5 shows the compensated longitudinal and transverse spectra for simulation II. The bottleneck is greatly diminished in $E_L(k)$ [Fig. 5(a), solid curve] which shows close to $k^{-5/3}$ scaling throughout the inertial range. In $E_T(k)$ [Fig. 5(b), solid curve], the bottleneck persists although its peak occurs slightly earlier in wave number than the bottleneck for the corresponding total spectrum. For completeness, we have also shown the 1D spectra compensated by $k^{4/3}$ [Fig. 5, dotted curves]. Based on our arguments above, we might have expected a stronger $k^{-4/3}$ scaling region of the transverse spectrum; such behavior is not clearly observed although there is a tendency towards a scaling shallower than $k^{-5/3}$ in the bottleneck regime. We plan in a future work to check the present indications that the bottleneck will be stronger in the transverse spectrum than in the longitudinal one because of the greater contamination of the former by the helical co-spectrum dynamics. This raises the intriguing possibility that τ_H affects the scaling of transverse structure functions, accounting for some of the observed difference between the scaling exponents of longitudinal and transverse structure functions in near-isotropic, high-Reynolds number turbulence data [15]. Such contributions would appear as parity breaking in the *isotropic* small scales, and might not be easily disentangled by, for example, the SO(3) group decomposition methods [see Ref. [16] and references therein] used to extract isotropic contributions to nonhelical turbulence statistics. Although this aspect of the influence of helicity dynamics remains speculative we hope this work provides sufficient motivation for further investigation.

The bottleneck is a well-known phenomenon which has been observed in experimental measurements [17,18] and Navier-Stokes simulations [19,20]. While the mean helicity of the flows in these investigations might be zero (although many do not report the mean helicity, using the often reasonable assumption that the flow is nonhelical on average), their
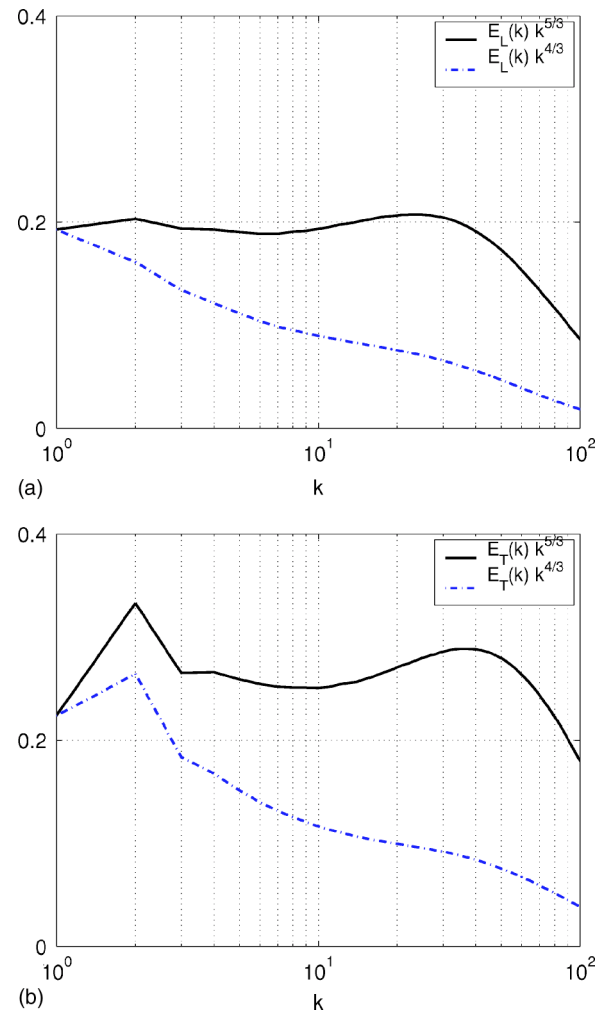

FIG. 5. Compensated (a) longitudinal and (b) transverse energy spectra for the simulation II. $E_L(k)$ shows a diminished bottleneck where the full spectrum $E(k)$ of Fig. 3(c) has a pronounced bottleneck. $E_T(k)$ shows a range of $k^{-5/3}$ coinciding with that of Fig. 3(c) and a persistent bottleneck with a scaling shallower than $k^{-5/3}$ scaling in the region of the bottleneck.

relative helicities might not be, and indeed have not been reported, because the connection between the Kolmogorov phenomenology, helicity dynamics, and the bottleneck did not exist. There have been various different approaches taken to explain this phenomenon, including viscous effects [21] and various kinematic arguments used to fit to a parametrized form [22–24]. What we are proposing here is a fundamental physical cause of the bottleneck due to the helicity dynamics slowing down the cascade of energy and helicity, the two conserved quantities in turbulence. Further, our empirical evidence, particularly in case II, where the total helicity is negligibly small, indicates that this effect could occur even in flows with essentially zero mean helicity but with nonzero relative helicity spectra [i.e., $H(k)$ is *not* zero everywhere]. Said differently, even if $\int H(k)dk=0$, there can be a range of k where $|H(k)|$ and hence $|H(k)|/2kE(k)$ is finite and possibly large enough that $\tau_E/\tau_H \sim [|H(k)|/2kE(k)]^{1/2}$ is not negligible. This effect was reported in an experimental work investigating spontaneous reflection-symmetry breaking in

boundary layer flows [11]. Such a scenario may occur since, while global helicity is statistically conserved in the inertial range, local helicity is not. Let $\xi(\mathbf{x})$ be the local helicity $\xi(\mathbf{x}) = \mathbf{u}(\mathbf{x}) \cdot \boldsymbol{\omega}(\mathbf{x})$. The equation for ξ reads

$$\partial_t \xi + u_j \partial_j \xi = -\partial_j(\omega_j p) + \tfrac{1}{2}\partial_j(\omega_j |\mathbf{u}|^2) + \nu[\nabla^2 \xi - 2(\partial_i u_j)(\partial_i \omega_j)]. \tag{11}$$

Locally, both the nonlinear and the viscous terms in the helicity dynamics might play a role in enhancing or diminishing the helicity. If the nonzero relative helicity in the scaling range arises from the nonlinear term, then the effects we see are indeed valid in the high-Reynolds number (inviscid) limit; if they arise from the viscous term then the effects we see would disappear at very high Reynolds numbers. This hypothesis is not testable at the present time but our work, which studies data from simulations which are similar to, or the same as, several performed before (see, for example, Refs. [8,25,26]), with comparable Reynolds number, gives substantial motivation to further examine these questions. We hope in particular to motivate measurements of the relative helicity and scaling behavior of the bottleneck region, in other flows which report the bottleneck phenomenon, in order to further check this connection.

We finally present a key result from analysis of the convergence of the dissipation integrals for a two-time-scale cascade. In Ref. [4] the same analysis was performed assuming a single time scale τ_E. The total dissipation of energy and helicity may be written as

$$D_E = 2\nu\left(\int_0^{k_c} dk \; k^2 E(k) + \int_{k_c}^{k_d} dk \; k^2 E(k)\right), \tag{12}$$

$$D_H = 2\nu\left(\int_0^{k_c} dk \; k^2 H(k) + \int_{k_c}^{k_d} dk \; k^2 H(k)\right), \tag{13}$$

where

$$E(k) = \begin{cases} C_E \varepsilon^{2/3} k^{-5/3} & \text{for} \quad k < k_c; \\ C_H \varepsilon h^{-1/3} k^{-4/3} & \text{for} \quad k_c < k < k_d, \end{cases} \tag{14}$$

$$H(k) = \begin{cases} c_E \varepsilon^{-1/3} k^{-5/3} & \text{for} \quad k < k_c; \\ c_H h^{2/3} k^{-4/3} & \text{for} \quad k_c < k < k_d, \end{cases} \tag{15}$$

and $C_E, C_H, c_E,$ and c_H are constants. The precise estimate of the transition wave number k_c is unimportant to what follows. The upper wave number k_d denotes the maximum beyond which the cascade is completely suppressed by viscosity. We obtain

$$D_E \sim \nu \; \varepsilon \; h^{-1/3} \; k_d^{5/3}, \tag{16}$$

$$D_H \sim \nu h^{2/3} k_d^{5/3}. \tag{17}$$

In Ref. [4] $k_d = k_\varepsilon \sim (\varepsilon/\nu^3)^{1/4}$ (the Kolmogorov dissipation wave number). In our case, setting $k_d = k_\varepsilon$ causes the integrals to diverge as $\nu^{-1/4}$ in the limit $\nu \to 0$. The choice $k_d \sim (h/\nu^3)^{1/5}$ ensures that the integrals converge to their correct values for the statistically steady state, $D_E = \varepsilon$ and $D_H = h$. We will call this new wave number k_h since it depends solely on the helicity dissipation rate. It must be distinguished from the k_H of Ref. [27] which depends on both energy and helicity dissipation rates. In the limit $\nu \to 0$, $k_\varepsilon \gg k_h$. In our simulations $k_\varepsilon > k_h$ by a factor of about 2.5. While in agreement with our analysis, we cannot really distinguish between the two wave numbers in these data. However, we suggest that the resolution requirement for measurements in turbulence with helicity, or more precisely, with nonzero helicity spectra, might be weaker than that in turbulence without helicity.

ACKNOWLEDGMENTS

[1] J. J. Moreau, C. R. Hebd. Seances Acad. Sci. **252**, 2810 (1961).

[2] H. K. Moffat, J. Fluid Mech. **35**, 117 (1969).

[3] A. Brissaud, U. Frisch, J. Leorat, M. Lesieur, and A. Mazure, Phys. Fluids **16**, 1366 (1973).

[4] Q. Chen, S. Chen, and G. L. Eyink, Phys. Fluids **15**, 361 (2003).

[5] R. H. Kraichnan, J. Fluid Mech. **47**, 525 (1971).

[6] R. Betchov, Phys. Fluids **4**, 925 (1961).

[7] S. Kurien, Physica D **175**, 167 (2003).

[8] M. Taylor, S. Kurien, and G. L. Eyink, Phys. Rev. E **68**, 026310 (2003).

[9] W. Polifke and L. Shtilman, Phys. Fluids A **1**, 2025 (1989).

[10] P. Constantin and A. Majda, Commun. Math. Phys. **115**, 435 (1988).

[11] M. Kholmyansky, M. Shapiro-Orot, and A. Tsinober, Proc. R.

Soc. London, Ser. A **457**, 2699 (2001).

[12] W. Dobler, N. E. L. Haugen, T. Yousef, and A. Brandenburg, Phys. Rev. E **68**, 026304 (2003).

[13] A. S. Monin and A. Yaglom, *Statistical Fluid Mechanics* (MIT Press, Cambridge, MA, 1987), Vol. 2.

[14] J. Andre and M. Lesieur, J. Fluid Mech. **81**, 187 (1977).

[15] K. R. Sreenivasan and B. Dhruva, Prog. Theor. Phys. Suppl. **103**, 103 (1998).

[16] S. Kurien and K. R. Sreenivasan, in *New Trends in Turbulence, Proceedings of the Les Houches Summer School 2000*, edited by M. Lesieur, A. Yaglom, and F. David (Springer-Verlag, Berlin, 2001), p. 53.

[17] K. Sreenivasan, Phys. Fluids **7**, 2778 (1995).

[18] S. Saddoughi and S. Veeravalli, J. Fluid Mech. **268**, 333 (1994).

[19] D. Martinez, S. Chen, G. Doolen, R. Kraichnan, L. Wang, and

Y. Zhou, J. Plasma Phys. **57**, 195 (1997).

[20] T. Gotoh, Comput. Phys. Commun. **147**, 530 (2002).

[21] G. Falkovich, Phys. Fluids **6**, 1411 (1994).

[22] Z. She and E. Jackson, Phys. Fluids A **5**, 1526 (1993).

[23] D. Lohse and A. Muller-Groeling, Phys. Rev. Lett. **74**, 1747 (1995).

[24] D. Lohse and A. Muller-Groeling, Phys. Rev. E **54**, 395 (1996).

[25] K. Sreenivasan, S. Vainshtein, R. Bhiladvala, I. SanGil, S. Chen, and N. Cao, Phys. Rev. Lett. **77**, 1488 (1996).

[26] T. Gotoh, D. Fukayama, and T. Nakano, Phys. Fluids **14**, 1065 (2002).

[27] P. D. Ditlevsen and P. Giuliani, Phys. Fluids **13**, 3508 (2001).